JACS Au
AN OPEN ACCESS JOURNAL OF THE AMERICAN CHEMICAL SOCIETY

pubs.acs.org/jacsau

Article

Operando Spectroscopic Study of the Dynamics of Ru Catalyst during Preferential Oxidation of CO and the Prevention of Ammonia Poisoning by Pt

Katsutoshi Sato,* Shuhei Zaitsu, Godai Kitayama, Sho Yagi, Yuto Kayada, Yoshihide Nishida, Yuichiro Wada, and Katsutoshi Nagaoka*

Cite This: *JACS Au* 2022, 2, 1627−1637

Read Online

ACCESS | Metrics & More | Article Recommendations | Supporting Information

ABSTRACT: Hydrogen is a promising clean energy source. In domestic polymer electrolyte fuel cell systems, hydrogen is produced by reforming of natural gas; however, the reformate contains carbon monoxide (CO) as a major impurity. This CO is removed from the reformate by a combination of the water−gas shift reaction and preferential oxidation of CO (PROX). Currently, Ru-based catalysts are the most common type of PROX catalyst; however, their durability against ammonia (NH_3) as an impurity produced in situ from trace amounts of nitrogen also contained in the reformate is an important issue. Previously, we found that addition of Pt to an Ru catalyst inhibited deactivation by NH_3. Here, we conducted operando XAFS and FT-IR spectroscopic analyses with simultaneous gas analysis to investigate the cause of the deactivation of an Ru-based PROX catalyst ($Ru/\alpha\text{-}Al_2O_3$) by NH_3 and the mechanism of suppression of the deactivation by adding Pt ($Pt/Ru/\alpha\text{-}Al_2O_3$). We found that nitric oxide (NO) produced by oxidation of NH_3 induces oxidation of the Ru nanoparticle surface, which deactivates the catalyst via a three-step process: First, NO directly adsorbs on Ru^0 to form $NO\text{-}Ru^{\delta+}$, which then induces the formation of $O\text{-}Ru^{n+}$ by oxidation of the surrounding Ru^0. Then, $O\text{-}Ru^{m+}$ is formed by oxidation of Ru^0 starting from the $O\text{-}Ru^{n+}$ nuclei and spreading across the surface of the nanoparticle. Pt inhibits this process by alloying with Ru and inducing the decomposition of adsorbed NO, which keeps the Ru in a metallic state.

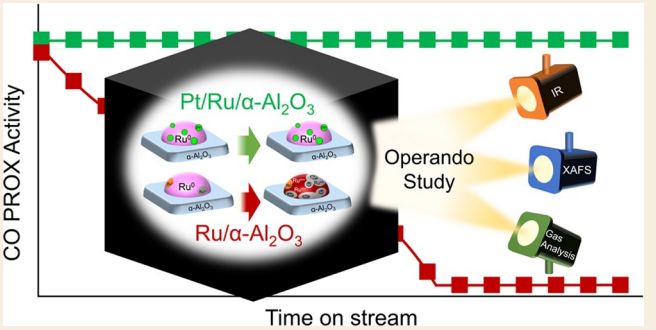

KEYWORDS: *hydrogen, clean energy, fuel cell, alloy catalyst, XAFS, ammonia*

INTRODUCTION

Reducing CO_2 emissions by using clean energy sources is an important step toward mitigating climate change. Hydrogen is a clean energy source that has attracted particular attention in recent years. Compared with conventional internal combustion engines, hydrogen fuel cells convert hydrogen into electric power with higher energy efficiency and with lower emissions of greenhouse gases. Therefore, polymer electrolyte fuel cells (PEFCs) are a promising technology for use as power generators for domestic use, portable use, and vehicles.[1,2] Currently, the most common means of producing hydrogen is the steam reforming of natural gas, the major component of which is methane.[3,4] However, although the reformate is hydrogen-rich, it also contains approximately 10% carbon monoxide (CO), which can poison the catalyst within the electrodes of PEFC stacks; therefore, the CO concentration must be reduced to below 10 ppm before supplying the reformate to the stacks.[5−7]

In domestic PEFC systems, CO is removed from the hydrogen-rich reformate by a two-stage process: first, the majority of the CO is removed by conversion to hydrogen and carbon dioxide via the water−gas shift reaction, and then the remaining CO is oxidized with air via preferential oxidation (PROX). PROX catalysts for use in domestic PEFC systems must have high activity, high selectivity for CO oxidation in the presence of excess hydrogen, and high durability against impurities, and they should be able to catalyze the oxidation reaction at low temperatures.[8−10] Previous studies have shown that metals such as Pt, Rh, Au, and Ru show high CO conversion performance and selectivity.[9−19] In particular, Ru exhibits high PROX performance over a wide temperature range and is relatively inexpensive compared with other noble metals[8,9] Therefore, although several potential non-noble

Received: March 27, 2022
Revised: April 27, 2022
Accepted: April 27, 2022
Published: May 9, 2022

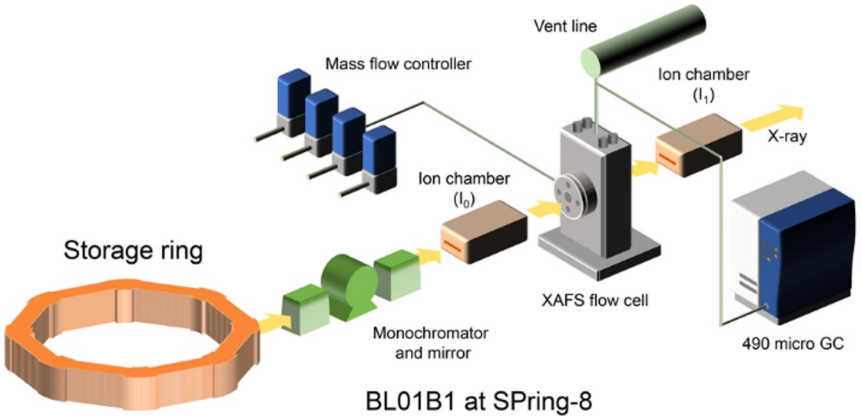

Figure 1. Schematic diagram of the operando XAFS set-up.

metal-based PROX catalysts have been reported,[20−28] Ru is still widely used as a PROX catalyst.[6,11]

The influence of impurities in the reformate on the catalytic activity and durability of PROX catalysts is an important topic of research.[29−33] For example, ammonia (NH_3) deactivates the conventional Ru-based PROX catalyst Ru/α-Al_2O_3. In domestic PEFC systems, natural gas is subjected to steam reforming, also over an Ru catalyst; however, these catalysts catalyze the synthesis of NH_3 from hydrogen and trace amounts of nitrogen that are also present in natural gas.[34,35] This results in the reformate containing NH_3 (usually 10−80 ppm) that deactivates the catalyst.[32,33]

Previously, we studied the activities of two Ru-based PROX catalysts, the conventional Ru-based PROX catalyst Ru/α-Al_2O_3 and a Pt−Ru bimetallic catalyst (Pt/Ru/α-Al_2O_3), in the presence of NH_3.[31] In the deactivated Ru/α-Al_2O_3 catalyst, we found that the Ru was partially oxidized. However, we also found that this oxidation was suppressed by the addition of a small amount of Pt (Pt/Ru = 1/17 mol/mol). Understanding more about the mechanism of deactivation of Ru catalysts by oxidation in the presence of NH_3 and the role Pt plays in suppressing this deactivation would provide useful insights for the design of advanced PROX catalysts.

In recent years, various operando spectroscopic techniques have been developed and used to observe the dynamics of catalysis under realistic conditions. The results obtained from these operando measurements have included valuable findings for designing improved catalysts. For example, operando X-ray absorption fine structure (XAFS) spectroscopy has excellent element selectively and has been used to examine the electronic state and local structure of trace metals within catalysts.[36−39] Similarly, operando infrared (IR) spectroscopy is useful for investigating surface-adsorbed species and for investigating the state of the catalyst surface, and this technique has been used to identify intermediates and poisons produced during various catalytic reactions.[18,39−41]

Here, we conducted operando XAFS and IR analyses to investigate the dynamics of Ru and Pt in two PROX catalysts, the conventional PROX catalyst Ru/α-Al_2O_3, and the bimetallic catalyst Pt/Ru/α-Al_2O_3. A combination of these analytical techniques with simultaneous gas analysis provided insights into the mechanism underlying the deactivation of Ru in the presence of NH_3 and the role Pt plays in suppressing this deactivation. We found that the NO produced from NH_3 is a poison that induces the oxidation of the surface of Ru nanoparticles via a three-step process: First, NO directly adsorbs on Ru^0 to form NO-$Ru^{\delta+}$, which then induces the formation of O-Ru^{n+} by oxidation of the surrounding Ru^0. Then, O-Ru^{m+} is formed by oxidation of Ru^0 starting from the O-Ru^{n+} nuclei ($m > n$) and spreading across the surface of the nanoparticle. Pt inhibits this process by alloying with Ru and inducing the decomposition of adsorbed NO, which keeps the Ru in a metallic state.

EXPERIMENTAL SECTION

Catalyst Preparation

Ru/α-Al_2O_3 catalyst and Pt/Ru/α-Al_2O_3 catalyst were prepared by means of an impregnation method with heating under air or helium flow. The Ru loading for Ru/α-Al_2O_3 was set to 2 wt %. Pt was sequentially impregnated into Ru/α-Al_2O_3, and the loading amount was set to 0.2 and 1.8 wt % for Pt and Ru, respectively (Pt/Ru = 1/17 mol/mol). Details of the preparation procedures are described in a previous report[31] and the Supporting Information.

Specific Surface Area Measurement

The specific surface areas of the catalysts after N_2 treatment at 300 °C were determined by using the Brunauer−Emmett−Teller method and a BELSORP-mini instrument (BEL Japan, Inc., Japan).

CO Chemisorption

CO chemisorption was measured by using the pulse injection method. The catalysts were reduced at 500 °C for 1 h under H_2 and cooled to room temperature under flowing He. CO was then pulsed over the catalysts, and CO uptake was measured with a thermal conductivity detector (GC-8A, Shimadzu, Japan).

HAADF-STEM Observation

High-angle annular dark-field scanning transmission electron microscopy (HAADF-STEM) images were obtained with a JEM-ARM200CF electron microscope (JEOL, Japan) operated at 120 kV. Samples were dispersed in ethanol under ambient conditions, and the dispersion was dropped onto a carbon-coated copper grid and then dried under a vacuum at ambient temperature for 24 h.

XAFS Spectroscopy

XAFS analyses of the Ru K and Pt L_3 adsorption edges were performed on the BL01B1 beamline at SPring-8 (Hyogo, Japan) with approval from the Japan Synchrotron Radiation Research Institute. An Si (111) and Si (311) double-crystal monochromator was used for the monochromation of X-rays. The catalyst samples were reduced under a flow of H_2 at 500 °C for 1 h in a glass reactor. After cooling in Ar, the catalyst samples were recovered from the glass reactor, crushed, pressed into a disk, and sealed in plastic bags filled with Ar. All the procedures for recovery, production of the sample disk, and transfer of the samples to the plastic bags were performed under Ar to avoid altering the samples through air exposure. The plastic bags were transferred to the beamline, and the spectra of the powdered catalysts

https://doi.org/10.1021/jacsau.2c00195
JACS Au 2022, 2, 1627−1637

were measured. The spectra of the Ru K-edges of the catalysts and reference samples were measured in transmittance mode using an ionization chamber. The spectra of the Pt L_3-edges of the catalysts were measured in fluorescence mode by using a Lytle detector.

Operando XAFS analyses were also performed on the BL01B1 beamline at SPring-8. The spectra were obtained in transmittance mode. Figure 1 provides a schematic diagram of the set up. Figure S1 provides an overview of a typical experimental procedure. A 100 mg sample of catalyst was placed in a XAFS flow cell (ASPEF-20-03, Kyowa Vacuum, Japan) reduced under H_2 flow at 500 °C for 1 h, allowed to cool to 110 °C under He flow, and then supplied with a mixed gas mimicking PROX conditions ($CO/O_2/He/H_2$ = 0.5/2.0/30.9/66.6) at a rate of 200 mL min^{-1}. To investigate the influence of NH_3, 200 ppm of NH_3 was added to the gas mixture. A gas chromatograph (490 micro GC, Agilent) was connected to the outlet of the XAFS cell and used to analyze the effluent gas. Data analysis was performed with the Athena and Artemis programs (ver. 0.9.25) included in the Demeter package.[42] A linear combination fitting analysis was performed using Ru/α-Al_2O_3 after reduction, which is in the metallic state, and RuO_2, which is in the oxidized state.

Fourier-Transform IR Spectroscopy

Operando IR analysis was performed by means of the transmission method and an FT-IR spectrometer (FT/IR-6600, JASCO) equipped with a mercury−cadmium−telluride detector. A 20 mg sample of catalyst powder was pressed into a disk (φ = 10 mm) and placed in a flow-type silica glass cell equipped with CaF_2 windows. The sample disk was then reduced at 500 °C for 1 h and cooled to 110 °C under He flow. IR spectra were obtained at 1 min intervals for 30 min under a flow of the gas mixture used in the operando XAFS experiment with or without the addition of NH_3.

RESULTS AND DISCUSSION

Physicochemical Properties of the Catalysts

Table 1 shows a comparison of the physicochemical properties of the Ru/α-Al_2O_3 and Pt/Ru/α-Al_2O_3 catalysts. Both catalysts showed the same specific surface area. HAADF-STEM observation of the catalyst surface morphology revealed that the metal nanoparticles were well dispersed over the support in both catalysts; however, the mean diameter of the metal nanoparticles was slightly larger in Ru/α-Al_2O_3 (2.8 nm) than in Pt/Ru/α-Al_2O_3 (2.1 nm) (Figure S2 and Table 1). Ru/α-Al_2O_3 showed slightly smaller CO chemisorption capacity on the metal surface, which is consistent with the HAADF-STEM observations. The size of metal nanoparticles and CO chemisorption capacities can be used as a measure of the number of active sites in a catalyst and therefore as indices of the activity of a catalyst; no marked differences in these parameters were observed between these two catalysts.

Table 1. Physicochemical Properties of the Catalysts

catalyst	specific surface area[a] (m^2 g^{-1})	mean Ru particle size[b] (nm)	CO/metal[c] (mol/mol)
Ru/α-Al_2O_3	10.0	2.8 ± 0.8	0.31
Pt/Ru/α-Al_2O_3	10.0	2.1 ± 0.5	0.33

[a]After reduction at 500 °C. [b]Estimated by HAADF-STEM. [c]Estimated from value of the CO chemisorption.

To study the local structure and electronic state of the Ru in the catalysts, X-ray absorption near-edge structure (XANES) and extended X-ray absorption fine structure (EXAFS) spectra of the Ru K-absorption edge of the reduced catalysts were obtained (Figure 2). Curve-fitting results are shown in Table S1. In the Ru K-edge XANES spectra of both catalysts, the shapes and positions of the peaks were comparable to those of Ru^0 powder (Figure 2a). In the k^3-weighted Fourier transforms of the EXAFS (FT-EXAFS) spectra of the Ru K-edge of both catalysts, a peak assigned to the Ru−Ru bond in a hexagonal close-packed arrangement was observed at around 2.7 Å, and no peak assignable to Ru−O was observed (Figure 2b). There were no significant differences in the electronic state and local structure between the two catalysts; we therefore concluded that reduction at 500 °C reduced the Ru in both catalysts to a metallic state.

Next, XANES and FT-EXAFS spectra of the Pt L_3-edge of Pt/Ru/α-Al_2O_3, 0.2 wt % Pt/α-Al_2O_3 monometal catalyst, and two reference materials after reduction at 500 °C were obtained (Figure 3). The height of the white line and the shape of the XANES spectrum of Pt/Ru/α-Al_2O_3 were comparable with those of the spectrum of Pt foil, indicating that the atomic Pt in the catalyst was in a metallic state (Figure 3a). In the k^3-weighted FT-EXAFS spectrum of the Pt L_3-edge of Pt/α-Al_2O_3, a peak assigned to the Pt−Pt bond in a face-centered cubic arrangement was observed at around 2.7 Å, and the coordination number of the Pt−Pt bond was determined to be 5.2 ± 0.15 (Figure S3a). In contrast, in the spectrum of Pt/Ru/α-Al_2O_3, no peak assignable to the Pt−Pt bond was observed, but a peak assignable to the Pt−metal bond, which is shorter than the Pt−Pt bond, was observed. Thus, we concluded that this Pt−metal bond was a Pt−Ru bond because the atomic radius of Ru is shorter than that of Pt.

Curve-fitting results are shown in Table S2. We assumed a crystallite model in which Pt dissolves within the hexagonal close-packed Ru structure to form an alloy. The bond distances were consistent with those of our assumed model (2.68 Å; Table S2). Such a short bond length indicates that atomic Pt formed an alloy with atomic Ru. However, the shape of the peak was not completely reproduced by our assumed model (Figure S3b). This difference in peak shape indicates that the Pt was not completely dissolved in the hexagonal close-packed Ru structure and that the crystal structure around the Pt was slightly distorted. In addition, the coordination number of the Pt−Ru bond in Pt/Ru/α-Al_2O_3 was much lower than that of the Ru−Ru bond in Pt/Ru/α-Al_2O_3 (2.6 ± 0.8 vs 9.7 ± 1.5), indicating that atomic Pt is abundant on the surface of the alloyed nanoparticles.

Activity Test and Operando XAFS Analysis

To clarify the behavior of the catalysts during the catalytic reaction, we carried out simultaneous operando XAFS and activity measurements under PROX conditions. Previously, we reported that the deactivation of Ru/α-Al_2O_3 in the presence of NH_3 is enhanced with increasing O_2/CO ratio.[31] Therefore, to emphasize the deactivation behavior of Ru/Al_2O_3 and the difference between Ru/α-Al_2O_3 and Pt/Ru/α-Al_2O_3, we carried out the operando study under flowing gas with CO/O_2 = 1/4 mol/mol. First, Ru/α-Al_2O_3 was examined (Figure 4). In the absence of NH_3, the conversions of CO and O_2 remained stable at 30−40% (Figure 4a). The indication was that some of the O_2 was consumed for not only CO oxidation but also H_2 oxidation. The XANES (Figure 4b) and k^3-weighted FT-EXAFS (Figure S4a) spectra remained largely unchanged. The changes in the state of the Ru in the catalyst were examined by linear combination fitting analysis of the Ru K-edge XANES spectrum, and we found that Ru remained in the metallic state throughout the measurement period (Figure 4a).

https://doi.org/10.1021/jacsau.2c00195
JACS Au 2022, 2, 1627−1637

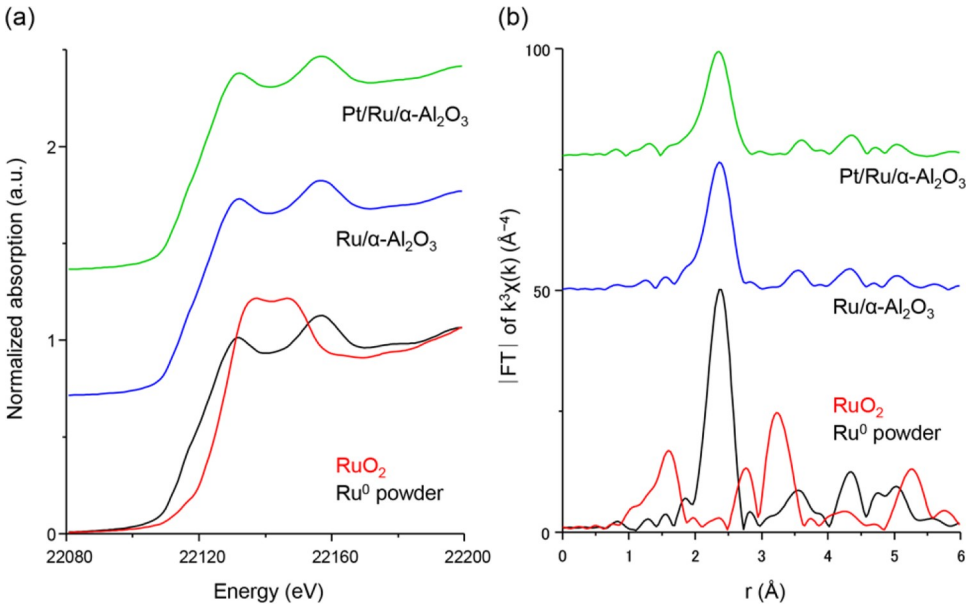

Figure 2. Ru K-edge XAFS spectra for Ru/α-Al_2O_3 and Pt/Ru/α-Al_2O_3 and for two reference materials. (a) XANES spectra and (b) k^3-weighted Fourier transforms of EXAFS spectra.

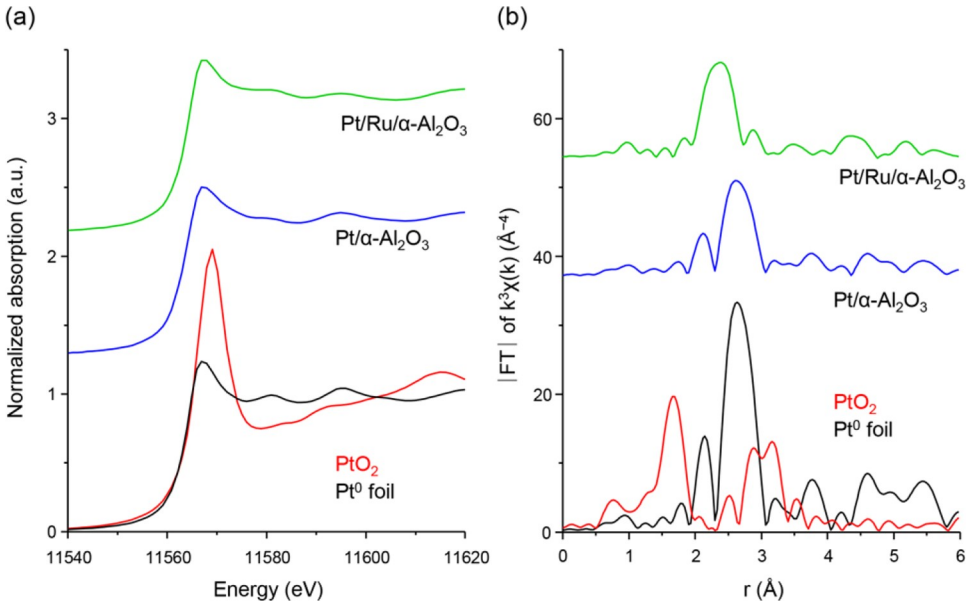

Figure 3. Pt L_3-edge XAFS spectra for Pt/Ru/α-Al_2O_3 and Pt/α-Al_2O_3 and for two reference materials. (a) XANES spectra and (b) k^3-weighted Fourier transforms of EXAFS spectra.

Next, 200 ppm of NH_3 was added to the mixed gas mixture, and its influence on catalytic behavior was examined (Figure 4c,d). Usually, reformate gas contains around 10−80 ppm of NH_3;[31,32] however, to emphasize the deactivation behavior of Ru/Al_2O_3, excess NH_3 was used in the present study. In the presence of NH_3, CO, and O_2, conversions were markedly reduced, with the curve following a sigmoidal shape. In the first 30 min of NH_3 supply, the conversions of CO and O_2 rapidly decreased from 30 to 17%. At 70 min, CO and O_2 conversions were almost 0% and remained at that value until the end of the analysis. The change in the ratio of metallic Ru species decreased in a similar sigmoidal manner. At 20 min after the start of NH_3 supply, the ratio of metallic Ru had decreased to around 75%, where it remained until 40 min, after which it decreased to around 65% until the end of analysis. In contrast, the change in the ratio of oxidized Ru species increased in a sigmoidal manner. At 65 min after the start of NH_3 supply, the ratio of oxidized Ru species had increased to around 35%, after which it remained constant until the end of analysis. These changes in the state of the Ru species suggest that the decrease of PROX activity of the Ru/α-Al_2O_3 catalyst in the presence of NH_3 is due to a change of the electronic state of the Ru. When the catalyst was completely deactivated, around 65% of the Ru remained in the metallic state and around 35% had been changed to an oxidized state, which is consistent with the ratio of atomic Ru exposed at the surface of the Ru nanoparticles as estimated by CO chemisorption measurement (Table 1). We thus concluded that the loss of catalytic activity of Ru/α-Al_2O_3 in the presence of NH_3 is due to oxidation of the Ru particle surface. In the FT-EXAFS spectrum of the Ru K-edge, the

https://doi.org/10.1021/jacsau.2c00195
JACS Au 2022, 2, 1627−1637

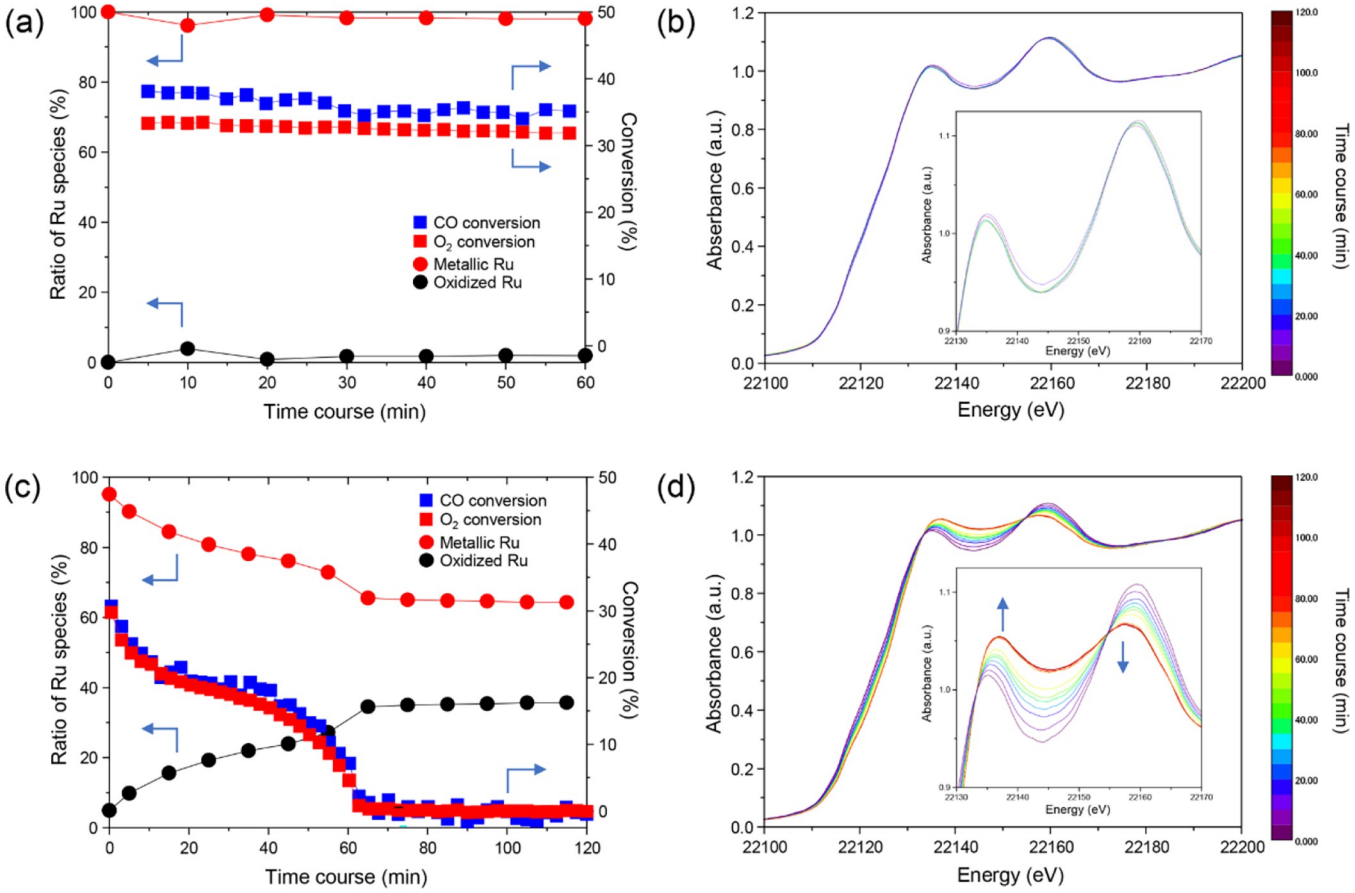

Figure 4. Time course of the Ru K-edge XANES spectra, CO and O_2 conversions, and Ru species ratios for Ru/α-Al_2O_3 during operando XAFS measurements in the absence (a, b) or presence (c, d) of NH_3.

intensity of the peak at around 2.6 Å assigned to the Ru−Ru bond decreased with time, whereas that of the peak at around 1.5 Å assigned to the Ru−O bond gradually increased (Figure S4b). At 70 min after the start of NH_3 supply, a strong contribution of Ru−Ru for FT-EXAFS spectra was still observable. These changes are consistent with the changes observed in the XANES spectra and provide further evidence that the change of the electronic state of Ru induced by NH_3 occurs only at the surface of the Ru particles.

Operando XAFS and activity measurements were also performed for Pt/Ru/α-Al_2O_3 (Figure 5). In the absence of NH_3, CO and O_2 conversions remained constant at around 45 and 38%, respectively (Figure 5a), the Ru K-edge XANES spectra did not change over time (Figure 5b), and the ratio of metallic Ru species remained constant (Figure 5a). In the presence of NH_3, the CO and O_2 conversions decreased only slightly (Figure 5c), unlike what was observed for Ru/α-Al_2O_3 (Figure 4c). In addition, the shapes of the XANES (Figure 5d) and FT-EXAFS (Figure S5) spectra changed only slightly, and the ratio of Ru metal species remained almost constant (Figure 5a). Taken together with the data obtained for Ru/α-Al_2O_3, these results indicate that the Ru in Pt/Ru/α-Al_2O_3 remains in the metallic state even in the presence of NH_3. Operando XAFS analysis of the Pt L_3-edge of Pt/Ru/α-Al_2O_3 showed no differences in the Pt L_3-edge XANES spectrum in the presence or absence of NH_3, which confirmed that the Pt also remained in the metallic state during the reaction (Figure S6). Thus, we conclude that the presence of metallic Pt suppresses the oxidation of Ru, which is the cause of deactivation of the Ru catalyst. As a result, Pt/Ru/Al_2O_3 maintains its PROX activity even in the presence of NH_3.

Operando IR

The preceding experiments show that the cause of the deactivation of Ru/α-Al_2O_3 is a change of the electronic state (i.e., oxidation) of metallic Ru induced by NH_3. However, NH_3 is a substance that is usually used as a reducing agent. For example, NH_3 is used for selective catalytic reduction of nitrogen oxide species in the exhaust purification systems of automobiles.[43] Therefore, we investigated the dynamics of the species adsorbed on the catalyst surface and the state of the nanoparticle surface by means of operando IR spectroscopy.

Figure 6 shows FT-IR spectra of Ru/α-Al_2O_3 and Pt/Ru/α-Al_2O_3 measured under a gas mixture mimicking PROX conditions in the absence of NH_3. In both spectra, peaks at around 2175 and 2120 cm^{-1} were assigned to absorption of gaseous CO. In the Ru/α-Al_2O_3 spectrum, the peak at 2024 cm^{-1} was assigned to linearly adsorbed CO on metallic Ru (Ru^0).[41,44] A shoulder peak derived from bridge-adsorbed CO on partially oxidized Ru ($Ru^{\delta+}$) was observed at around 1990 cm^{-1}.[45−47] A small peak at 2056 cm^{-1} was assigned to dicarbonyl CO species adsorbed on Ru^{n+}.[47] These results suggest that under PROX conditions, part of the Ru nanoparticle surface is oxidized and that the extent of this oxidation is too slight to be observed by XAFS. We assume that atomic Ru (e.g., Ru at vertex and edge sites on the catalyst surface), which is particularly sensitive to oxygen, may be oxidized even in the absence of NH_3. In the Pt/Ru/α-Al_2O_3

https://doi.org/10.1021/jacsau.2c00195
JACS Au 2022, 2, 1627−1637

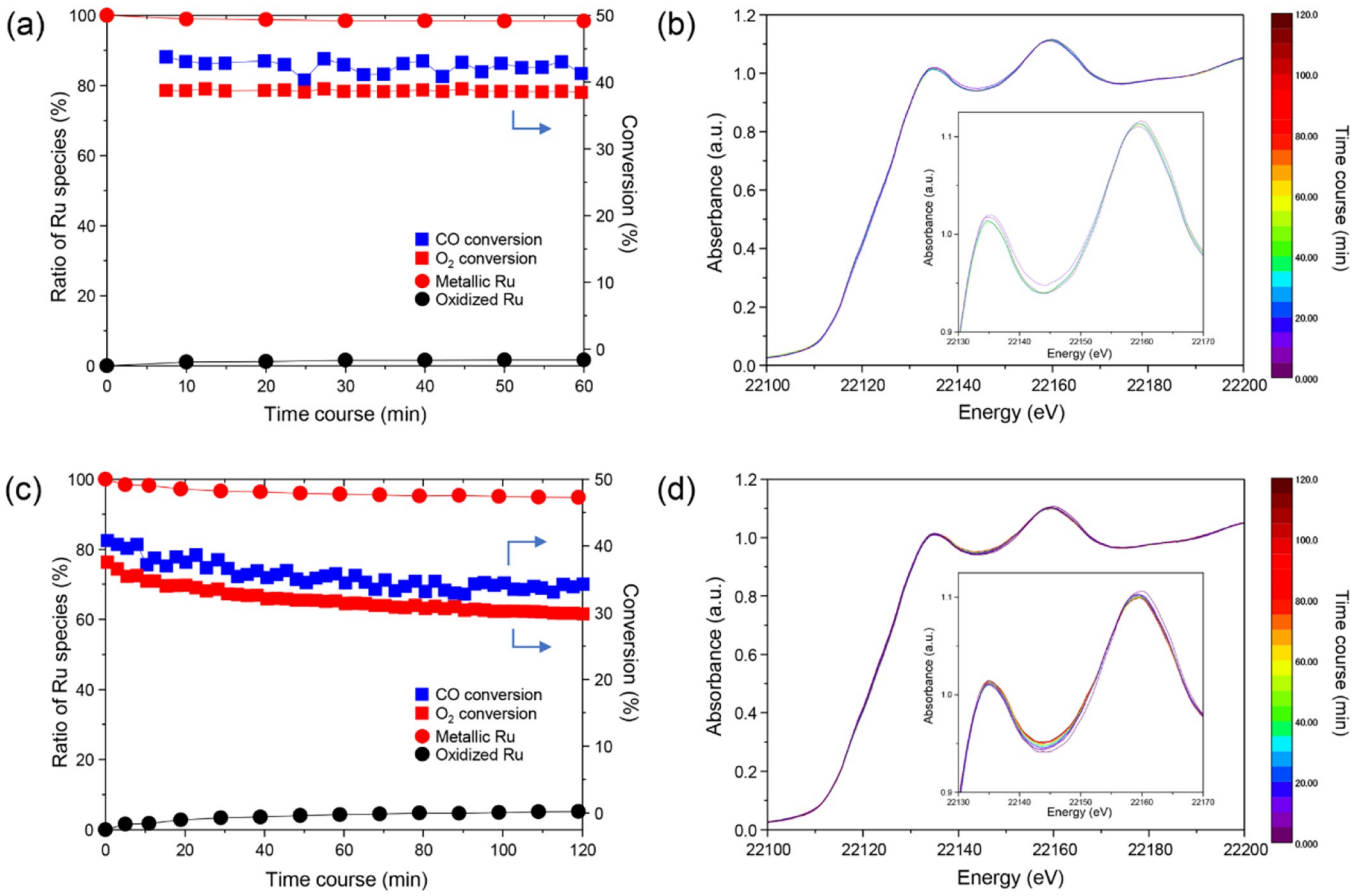

Figure 5. Time course of the Ru K-edge XANES spectra, CO and O_2 conversions, and Ru species ratios for Pt/Ru/α-Al_2O_3 during operando XAFS measurements in the absence (a, b) or presence (c, d) of NH_3.

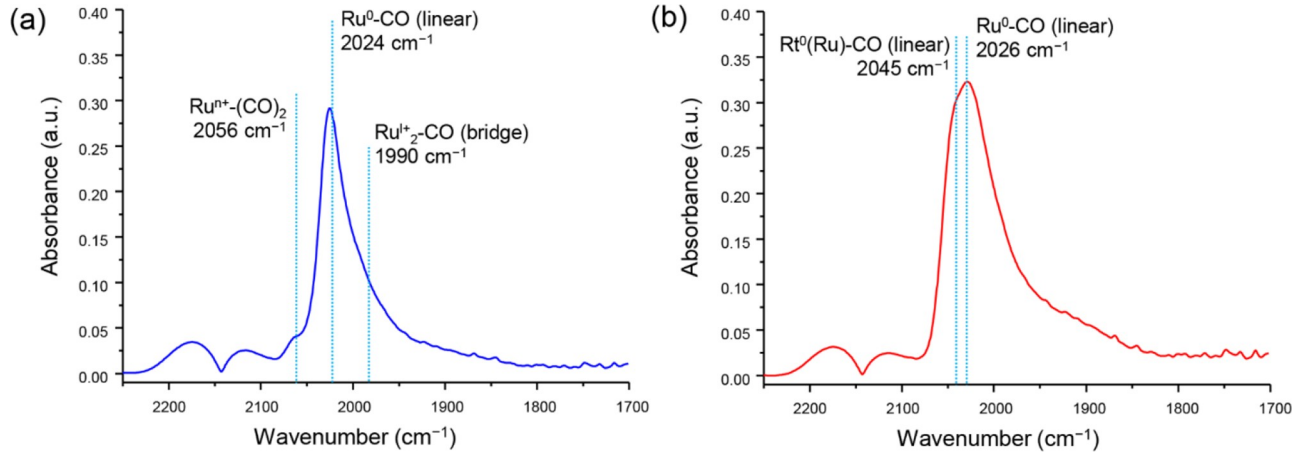

Figure 6. Difference IR spectra obtained under a flowing gas mixture mimicking PROX at 110 °C on Ru/α-Al_2O_3 (a) and Pt/Ru/α-Al_2O_3 (b).

spectrum, a peak assigned to linearly adsorbed CO on Ru^0 was observed at 2026 cm^{-1}, which is consistent with the peak position in the Ru/α-Al_2O_3 spectrum. It is reported that a peak assignable to linear CO adsorbed on Pt^0 appears at 2080 cm^{-1}.[14,41] Although no peak was observed at that wavenumber, a small shoulder was observed at a lower wavenumber (2045 cm^{-1}). This shoulder was assigned to linearly adsorbed CO on Pt^0 alloying with Ru with lower electron negativity compared with Pt, with the rationale being that the Pt donates an electron to the antibonding π orbital of C−O bond, the C−O bond is weakened, and the peak position is shifted to a lower wavenumber.

The changes in the difference IR spectrum of Ru/α-Al_2O_3 over time were examined after NH_3 was added to the gas mixture (Figure 7a,c). In the first 4 min after the introduction of NH_3, the peak assigned to nitrosyl species (NO) produced by oxidation of NH_3 and adsorbed on $Ru^{\delta+}$ (1840 cm^{-1}; Figure S7a) increased.[48] At the same time, the intensity of the peak assigned to dicarbonyl CO species adsorbed on Ru^{n+} (2050 cm^{-1}) also increased and that of the peak assigned to linearly adsorbed CO on Ru^0 decreased, with the rate of decrease of

https://doi.org/10.1021/jacsau.2c00195
JACS Au 2022, 2, 1627−1637

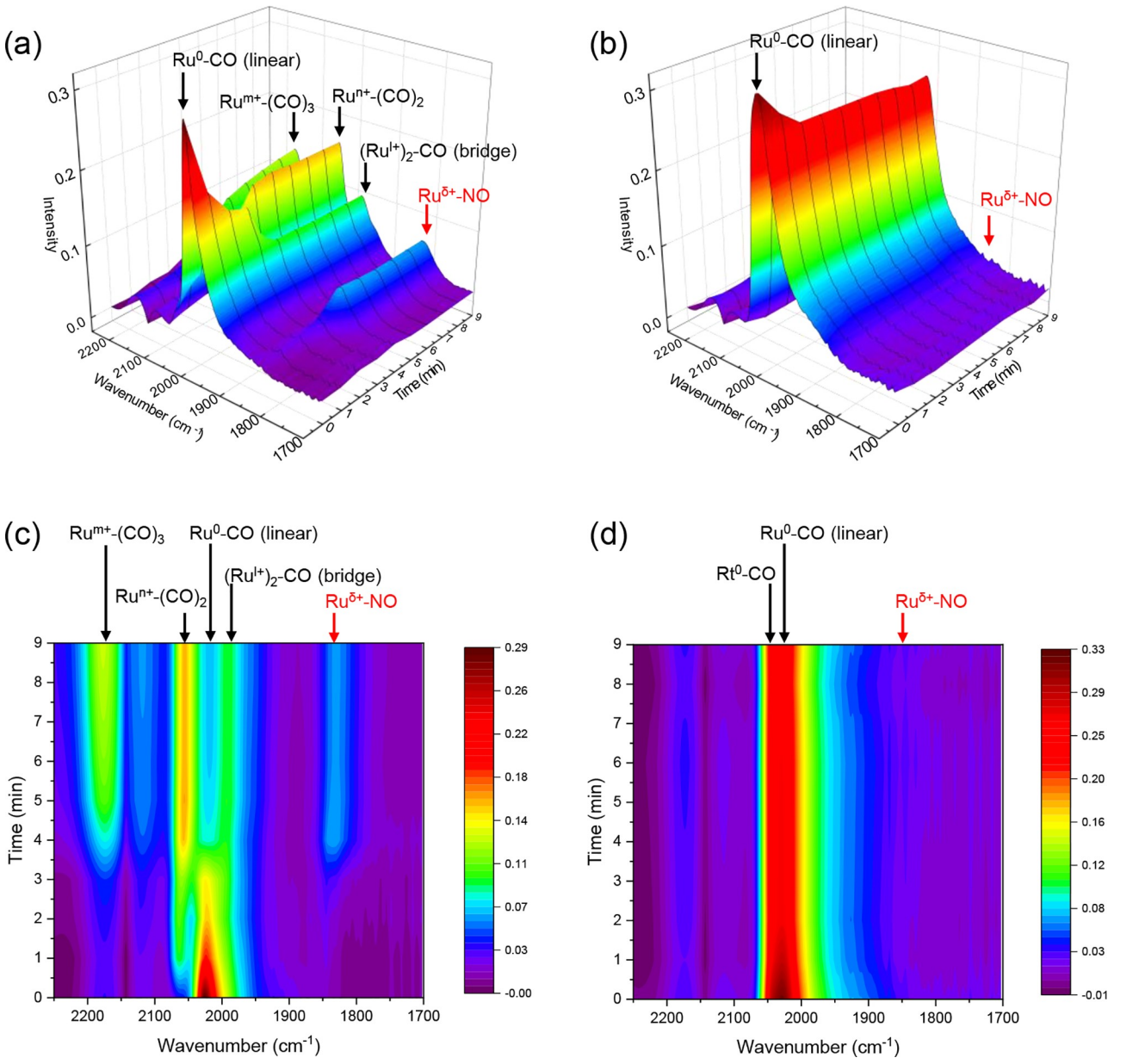

Figure 7. Changes of the difference IR spectra obtained with a flowing gas mixture mimicking PROX conditions at 110 °C over Ru/α-Al_2O_3 (a, c) and Pt/Ru/α-Al_2O_3 (b, d). Three-dimensional plots (a, d) and contour plots (c, d).

the peak intensity decreasing with time. These results suggest that the number of Ru^0 sites, which are the active sites of the PROX reaction, decreased over time because of oxidation of Ru^0 to $Ru^{\delta+}$ and Ru^{n+} by adsorption of NO. Interaction between adsorbed CO species and electron-poor Ru species ($Ru^{\delta+}$ and Ru^{n+}) is weak, and therefore, these species are not converted to CO_2. After the 4 min timepoint, the peak at 2180 cm^{-1} assigned to tricarbonyl CO adsorbed on Ru^{m+}, which has lower electron density compared to Ru^{n+} ($m > n$), increased in conjunction with decreases of the peak assigned to linear CO adsorbed on Ru^0.[44,49] The rate of decrease of the peak intensity increased with time. In contrast, the intensity of the peaks assigned to NO-$Ru^{\delta+}$ and dicarbonyl CO adsorbed on Ru^{n+} did not change during this period. Together, these results suggest that the number of Ru^0 sites decreases due to their oxidation to Ru^{m+}. Here, it should be noted that irrespective of whether NH_3 was present or not, almost no change was observed in the peak at about 1990 cm^{-1}, which was assigned to bridge CO adsorbed on Ru^{l+}. The interaction between bridge CO and Ru^{l+} is stronger than that of linear CO on Ru^0; therefore, it is considered that bridge CO does not participate in the reaction pathway of PROX under these low-temperature conditions. Also note that the observed changes of peak intensity were rapid and had finished within 10 min because the space velocity used for the operando IR measurements (600,000 mL h^{-1} g^{-1}) was much larger than that used for the operando XAFS measurements (120,000 mL h^{-1} g^{-1}).

In the Pt/Ru/α-Al_2O_3 spectrum (Figure 7b,d), the intensity of the peak assigned to NO adsorbed on $Ru^{\delta+}$ was much weaker than that in the Ru/α-Al_2O_3 spectrum (Figure S7). This suggests that the formation and/or adsorption of NO is inhibited over Pt/Ru/α-Al_2O_3. In the presence of NH_3, the intensity of the peak attributed to linearly adsorbed CO on Ru^0 decreased slightly within the first few minutes after the start of

https://doi.org/10.1021/jacsau.2c00195
JACS Au 2022, 2, 1627−1637

NH_3 addition but remained constant thereafter. In addition, there was only a slight change in the intensity of the peak assigned to linearly adsorbed CO on Pt. These results show that the surface Ru^0 was maintained even in the presence of NH_3. We thus conclude that Pt suppresses the change of the electronic state of Ru induced by the adsorption of NO species, which inhibits catalyst deactivation.

Mechanism of the Deactivation of Ru/α-Al_2O_3 and the Effect of Pt Addition

Based on the above results, we considered the mechanism of the deactivation of Ru/α-Al_2O_3 induced by NH_3 and the role Pt plays in suppressing this deactivation. In the presence of NH_3, over both catalysts, NH_3 reacts with oxygen in the gas mixture at the Ru surface and is oxidized to NO, and it is this NO species that deactivates the catalyst. We previously reported that the conversion of 130 ppm of NH_3 in the gas mixture was less than 30% and that the effluent gas included trace amounts of NO_x over Ru/α-Al_2O_3.[31] A trace amount of NO_2 was detected in the effluent gas in our previous study; therefore, we surmised that NO_2 is related to deactivation of the Ru catalyst. However, during the operando IR investigation in the present study, no adsorption peaks assignable to NO_2 were observed. We thus conclude that the NO_2 observed in our previous study was probably produced by a non-catalytic reaction between NO and O_2 downstream of the catalyst bed and that it is NO rather than NO_2 that induces the deactivation of the catalyst.

In the Ru/α-Al_2O_3 catalyst, a three-step change of the electronic state of Ru observed using IR analyses is in agreement with the time-course operando XAFS measurements. We consider that these changes of the electronic state of Ru are induced by the strong electron-withdrawing ability of NO. Based on the present results, we propose the following three-step mechanism of the deactivation mechanism of Ru/α-Al_2O_3 catalyst (Figure 8). In the first step, at the beginning of NH_3 addition (Figure 8b), NO adsorbs directly on Ru^0 and changes the electronic state of Ru from metallic to oxidic ($Ru^{\delta+}$), which causes rapid oxidation of the surrounding Ru^0 to Ru^{n+} and an exponential decrease of the number of Ru^0 sites, which decreases the CO oxidation ability of the catalyst.

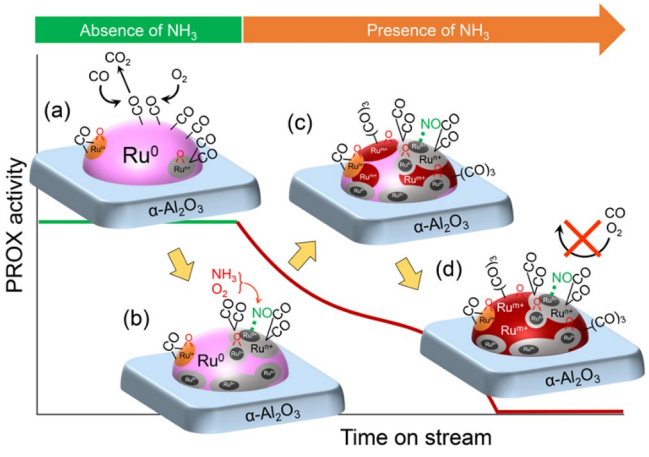

Figure 8. Proposed mechanism of the deactivation of Ru/α-Al_2O_3 in the presence of NH_3. Schematic illustration of Ru/α-Al_2O_3 under PROX conditions in the absence of NH_3 (a), at the beginning of NH_3 addition (b), during the spread of surface oxidation (c), and in the resultant state (d).

During this step, as suggested by our XANES analysis, about 25% of the metallic Ru is changed to the oxidic state, which is about 75% of the atomic Ru exposed on the Ru nanoparticle surface. In the second step, the remaining Ru^0, which is around 25% of the exposed atomic Ru, is oxidized to an electron-poor state (Ru^{m+}), and this oxidation spreads from the O-Ru^{n+} nuclei across the nanoparticle surface, resulting in a decrease of activity that follows a reverse sigmoid curve (Figure 8c). Finally, when all of the exposed Ru atoms have been oxidized, the PROX activity of the Ru/α-Al_2O_3 catalyst is lost (Figure 8d).

In contrast, the behavior of NO species over Pt/Ru/α-Al_2O_3 is completely different from that over Ru/α-Al_2O_3 (Figure 9).

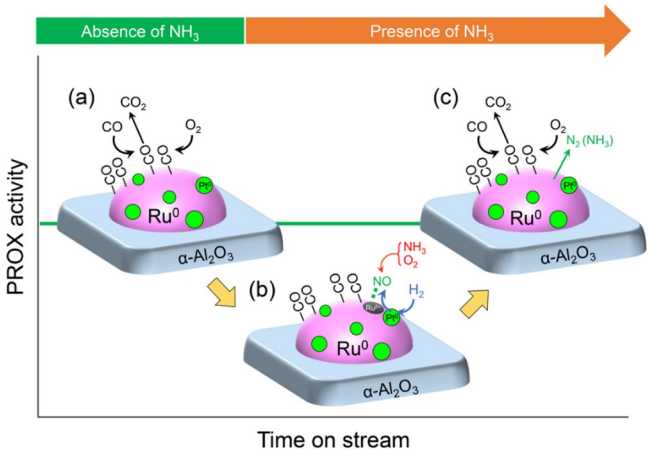

Figure 9. Proposed mechanism of the effect of Pt in Pt/Ru/α-Al_2O_3. Schematic illustration of Pt/Ru/α-Al_2O_3 under PROX conditions in the absence of NH_3 (a), during maintenance of the surface metallic state (b), and during maintenance of PROX activity in the presence of NH_3 (c).

As shown in Figure S7, the intensity of the peak assignable to adsorbed NO over Pt/Ru/α-Al_2O_3 is much smaller than that for Ru/α-Al_2O_3. This indicates that Pt induces rapid decomposition of NO species after their adsorption on the alloy nanoparticle surface (Figure 9b). Pt is a well-known catalyst of selective catalytic reduction with H_2.[50] Pt catalysts reduce NO by using H_2 as a reducing agent even in the presence of O_2 and at a similar temperature range as that used for PROX. Therefore, it is assumed that NO is also efficiently decomposed over Pt under PROX conditions. In addition, Pt promotes H_2 dissociation and activation, as has been previously reported and termed the "spillover effect."[51] Such activated hydrogen species show good reducing ability. XAFS revealed that the major fraction of Pt forms an alloy at the Ru nanoparticle surface. Therefore, in the presence of even trace amounts of Pt (Pt/Ru = 1/17 mol/mol), activated hydrogen is supplied from the Pt to the Ru nanoparticle surface, which promotes the reduction of Ru. Therefore, the surface of the Ru nanoparticle is maintained in a metallic state, and the deactivation of the catalyst is suppressed (Figure 9c).

CONCLUSIONS

Here, we directly observed the dynamics of Ru species in Ru/α-Al_2O_3 and Pt/Ru/α-Al_2O_3 PROX catalysts under conditions simulating those used in domestic PEFC systems by using operando spectroscopic techniques with simultaneous gas analysis. Based on these analyses, we obtained insights into the

https://doi.org/10.1021/jacsau.2c00195
JACS Au 2022, 2, 1627−1637

causes of catalyst deactivation by NH_3 and the effect of Pt in suppressing this deactivation. We found that the deactivation of Ru catalyst is caused by adsorption of NO species produced from NH_3. Due to its strong electron-withdrawing character, this adsorbed NO induces a change of the electronic state of atomic Ru at the Ru nanoparticle surface in three steps. In the first step, NO directly adsorbs on Ru^0 to form NO-$Ru^{\delta+}$, which then induces the formation of O-Ru^{n+} by oxidation of the surrounding Ru^0. Then, O-Ru^{m+} is formed by oxidation of Ru^0 starting from the O-Ru^{n+} nuclei ($m > n$) and spreading across the surface of the nanoparticle. Pt inhibits this process by alloying with Ru and inducing the decomposition of adsorbed NO, which keeps the Ru in a metallic state, suppresses oxidation of the Ru nanoparticle surface, and prevents deactivation of the catalyst. To the best of our knowledge, this is the first example of an operando spectroscopy investigation of the mechanism of PROX catalyst deactivation. We believe that the uncovered dynamics of surface Ru and Pt species based on operando analysis will not only contribute to the development of a highly durable PROX catalyst but also lead to the novel design of composite metal catalysts.

■ ASSOCIATED CONTENT

Supporting Information

The Supporting Information is available free of charge at https://pubs.acs.org/doi/10.1021/jacsau.2c00195.

Procedure of catalyst preparation; procedure for operando XAFS measurement; STEM images and particle size distributions; additional XAFS spectra; results of curve-fitting analysis; extended IR spectra (PDF)

■ AUTHOR INFORMATION

Corresponding Authors

Katsutoshi Sato − *Department of Chemical Systems Engineering, Graduate school of Engineering, Nagoya University, Nagoya 464-8603, Japan; Elements Strategy Initiative for Catalysts and Batteries, Kyoto University, Kyoto 615-8245, Japan;* orcid.org/0000-0002-3998-7012; Email: sato.katsutoshi@material.nagoya-u.ac.jp

Katsutoshi Nagaoka − *Department of Chemical Systems Engineering, Graduate school of Engineering, Nagoya University, Nagoya 464-8603, Japan; Elements Strategy Initiative for Catalysts and Batteries, Kyoto University, Kyoto 615-8245, Japan;* orcid.org/0000-0003-1774-1537; Email: nagaoka.katsutoshi@material.nagoya-u.ac.jp

Authors

Shuhei Zaitsu − *Department of Applied Chemistry, Graduate School of Engineering, Oita University, Oita 870−1192, Japan*

Godai Kitayama − *Department of Applied Chemistry, Graduate School of Engineering, Oita University, Oita 870−1192, Japan*

Sho Yagi − *Department of Applied Chemistry, Graduate School of Engineering, Oita University, Oita 870−1192, Japan*

Yuto Kayada − *Department of Applied Chemistry, Graduate School of Engineering, Oita University, Oita 870−1192, Japan*

Yoshihide Nishida − *Department of Chemical Systems Engineering, Graduate school of Engineering, Nagoya University, Nagoya 464-8603, Japan;* Present Address: Advanced Ceramics Research Center, Nagoya Institute of Technology, 10−6-29 Asahigaoka, Tajimi, Gifu 507−0071, Japan

Yuichiro Wada − *Department of Integrated Science and Technology, Faculty of Science and Technology, Oita University, Oita 870−1192, Japan*

Complete contact information is available at: https://pubs.acs.org/10.1021/jacsau.2c00195

Notes

The authors declare no competing financial interest.

■ ACKNOWLEDGMENTS

This work was managed by the Elements Strategy Initiative for Catalysts and Batteries, which is supported by the Japanese Ministry of Education, Culture, Sports, Science and Technology. XAFS measurements were performed at the BL01B1 public beamline of SPring-8 (Hyogo, Japan) with approval from the Japan Synchrotron Radiation Research Institute (JASRI; proposal no. 2013B1771, 2014B1824, and 2019A1379). We thank Dr. T. Ina and Mr. K. Kato (JASRI) for their kind support with the XAFS measurements. We thank Prof. K. Teramura and Dr. H. Asakura (Kyoto University) for their fruitful discussions concerning X-ray absorption analysis. We also thank T. Yamamoto, T. Toriyama, and Prof. S. Matsumura (Kyushu University) for the STEM analysis.

■ REFERENCES

(1) Rabis, A.; Rodriguez, P.; Schmidt, T. J. Electrocatalysis for Polymer Electrolyte Fuel Cells: Recent Achievements and Future Challenges. *ACS Catal.* **2012**, *2*, 864−890.

(2) Mehta, V.; Cooper, J. S. Review and analysis of PEM fuel cell design and manufacturing. *J. Power Sources* **2003**, *114*, 32−53.

(3) Mohanty, U. S.; Ali, M.; Azhar, M. R.; Al-Yaseri, A.; Keshavarz, A.; Iglauer, S. Current advances in syngas (CO + H_2) production through bi-reforming of methane using various catalysts: A review. *Int. J. Hydrogen Energy* **2021**, *46*, 32809−32845.

(4) Meloni, E.; Martino, M.; Palma, V. A Short Review on Ni Based Catalysts and Related Engineering Issues for Methane Steam Reforming. *Catalysts* **2020**, *10*, 352.

(5) Choudhary, T.; Goodman, D. W. CO-free fuel processing for fuel cell applications. *Catal. Today* **2002**, *77*, 65−78.

(6) Echigo, M.; Inaya, A.; Shinke, N.; Hirai, K.; Tabata, T. Ten-Year Durability of a High-Performance CO Preferential Oxidation Catalyst for Residential Polymer Electrolyte Fuel Cell Systems. *J. Chem. Eng. Jpn.* **2020**, *53*, 64−67.

(7) Garcia, A. C.; Paganin, V. A.; Ticianelli, E. A. CO tolerance of PdPt/C and PdPtRu/C anodes for PEMFC. *Electrochim. Acta* **2008**, *53*, 4309−4315.

(8) Jing, P.; Gong, X.; Liu, B.; Zhang, J. Recent advances in synergistic effect promoted catalysts for preferential oxidation of carbon monoxide. *Catal. Sci. Technol.* **2020**, *10*, 919−934.

(9) Liu, K.; Wang, A.; Zhang, T. Recent Advances in Preferential Oxidation of CO Reaction over Platinum Group Metal Catalysts. *ACS Catal.* **2012**, *2*, 1165−1178.

(10) Lin, J.; Wang, X.; Zhang, T. Recent progress in CO oxidation over Pt-group-metal catalysts at low temperatures. *Chin. J. Catal.* **2016**, *37*, 1805−1813.

(11) Echigo, M.; Shinke, N.; Takami, S.; Tabata, T. Performance of a natural gas fuel processor for residential PEFC system using a novel CO preferential oxidation catalyst. *J. Power Sources* **2004**, *132*, 29−35.

(12) Chin, S. Y.; Alexeev, O. S.; Amiridis, M. D. Preferential oxidation of CO under excess H conditions over Ru catalysts. *Appl. Catal., A* **2005**, *286*, 157−166.

(13) Chin, S.; Alexeev, O.; Amiridis, M. Structure and reactivity of Pt−Ru/SiO_2 catalysts for the preferential oxidation of CO under excess H_2. *J. Catal.* **2006**, *243*, 329−339.
(14) Kuriyama, M.; Tanaka, H.; Ito, S.; Kubota, T.; Miyao, T.; Naito, S.; Tomishige, K.; Kunimori, K. Promoting mechanism of potassium in preferential CO oxidation on Pt/Al_2O_3. *J. Catal.* **2007**, *252*, 39−48.
(15) Alayoglu, S.; Nilekar, A. U.; Mavrikakis, M.; Eichhorn, B. Ru-Pt core-shell nanoparticles for preferential oxidation of carbon monoxide in hydrogen. *Nat. Mater.* **2008**, *7*, 333−338.
(16) Perkas, N.; Teo, J.; Shen, S.; Wang, Z.; Highfield, J.; Zhong, Z.; Gedanken, A. Supported Ru catalysts prepared by two sonication-assisted methods for preferential oxidation of CO in H_2. *Phys. Chem. Chem. Phys.* **2011**, *13*, 15690−15698.
(17) Hernández, J. A.; Gómez, S. A.; Zepeda, T. A.; Fierro-González, J. C.; Fuentes, G. A. Insight into the Deactivation of Au/CeO_2 Catalysts Studied by In Situ Spectroscopy during the CO-PROX Reaction. *ACS Catal.* **2015**, *5*, 4003−4012.
(18) Chen, X.; Delgado, J. J.; Gatica, J. M.; Zerrad, S.; Cies, J. M.; Bernal, S. Preferential oxidation of CO in the presence of excess of hydrogen on Ru/Al_2O_3 catalyst: Promoting effect of ceria−terbia mixed oxide. *J. Catal.* **2013**, *299*, 272−283.
(19) Du, X.; Lang, Y.; Cao, K.; Yang, J.; Cai, J.; Shan, B.; Chen, R. Bifunctionally faceted Pt/Ru nanoparticles for preferential oxidation of CO in H_2. *J. Catal.* **2021**, *396*, 148−156.
(20) Xie, Y.; Wu, J.; Jing, G.; Zhang, H.; Zeng, S.; Tian, X.; Zou, X.; Wen, J.; Su, H.; Zhong, C.-J.; Cui, P. Structural origin of high catalytic activity for preferential CO oxidation over CuO/CeO_2 nanocatalysts with different shapes. *Appl. Catal., B* **2018**, *239*, 665−676.
(21) Cao, L.; Liu, W.; Luo, Q.; Yin, R.; Wang, B.; Weissenrieder, J.; Soldemo, M.; Yan, H.; Lin, Y.; Sun, Z.; Ma, C.; Zhang, W.; Chen, S.; Wang, H.; Guan, Q.; Yao, T.; Wei, S.; Yang, J.; Lu, J. Atomically dispersed iron hydroxide anchored on Pt for preferential oxidation of CO in H_2. *Nature* **2019**, *565*, 631−635.
(22) Davó-Quiñonero, A.; Bailón-García, E.; López-Rodríguez, S.; Juan-Juan, J.; Lozano-Castelló, D.; García-Melchor, M.; Herrera, F. C.; Pellegrin, E.; Escudero, C.; Bueno-López, A. Insights into the Oxygen Vacancy Filling Mechanism in CuO/CeO_2 Catalysts: A Key Step Toward High Selectivity in Preferential CO Oxidation. *ACS Catal.* **2020**, *10*, 6532−6545.
(23) Nyathi, T. M.; Fadlalla, M. I.; Fischer, N.; York, A. P. E.; Olivier, E. J.; Gibson, E. K.; Wells, P. P.; Claeys, M. Support and gas environment effects on the preferential oxidation of carbon monoxide over Co_3O_4 catalysts studied in situ. *Appl. Catal., B* **2021**, *297*, No. 120450.
(24) Zhong, L.; Barreau, M.; Chen, D.; Caps, V.; Haevecker, M.; Teschner, D.; Simonne, D. H.; Borfecchia, E.; Baaziz, W.; Šmíd, B.; Zafeiratos, S. Effect of manganese promotion on the activity and selectivity of cobalt catalysts for CO preferential oxidation. *Appl. Catal., B* **2021**, *297*, No. 120397.
(25) Davo-Quinonero, A.; Lopez-Rodriguez, S.; Bailon-Garcia, E.; Lozano-Castello, D.; Bueno-Lopez, A. Mineral Manganese Oxides as Oxidation Catalysts: Capabilities in the CO-PROX Reaction. *ACS Sustainable Chem. Eng.* **2021**, *9*, 6329−6336.
(26) Chagas, C. A.; Schmal, M. The effect of copper oxide on the CuO−NiO/CeO_2 structure and its influence on the CO-PROX reaction. *Int. J. Hydrogen Energy* **2022**, *47*, 8858−8866.
(27) Liu, Y.; Zhang, A.; Xue, L.; Zhang, H.; Hao, Y.; Wang, Y.; Wu, J.; Zeng, S. Dual Active Sites of CO Adsorption and Activation over PtCu Alloy Nanocages for Preferential Oxidation of Carbon Monoxide. *ACS Appl. Energy Mater.* **2021**, *5*, 604−614.
(28) Fiuza, T. E. R.; Zanchet, D. Supported AuCu Alloy Nanoparticles for the Preferential Oxidation of CO (CO-PROX). *ACS Appl. Nano Mater.* **2019**, *3*, 923−934.
(29) Nyathi, T. M.; Fischer, N.; York, A. P. E.; Claeys, M. Environment-Dependent Catalytic Performance and Phase Stability of Co_3O_4 in the Preferential Oxidation of Carbon Monoxide Studied In Situ. *ACS Catal.* **2020**, *10*, 11892−11911.
(30) Alzahrani, F.; Rusi, H.; Assabumrungrat, S.; Fernandes, D. L. A.; Aiouache, F. Deactivation of the preferential oxidation of CO in packed bed reactor by 3D modelling and near-infrared tomography. *Chem. Eng. J.* **2019**, *378*, No. 122082.
(31) Sato, K.; Yagi, S.; Zaitsu, S.; Kitayama, G.; Kayada, Y.; Teramura, K.; Takita, Y.; Nagaoka, K. Inhibition of ammonia poisoning by addition of platinum to Ru/α-Al_2O_3 for preferential CO oxidation in fuel cells. *ChemSusChem* **2014**, *7*, 3264−3267.
(32) Wakita, H.; Ukai, K.; Takeguchi, T.; Ueda, W. Deactivation of Ru/Al_2O_3 Catalyst for Preferential CO Oxidation in the Presence of Low-concentration NH_3 by Nitrosyl Species. *Chem. Lett.* **2006**, *35*, 734−735.
(33) Wakita, H.; Ukai, K.; Takeguchi, T.; Ueda, W. Mechanistic Investigation of Deactivation of Ru/Al_2O_3 Catalyst for Preferential CO Oxidation in the Presence of NH_3. *J. Phys. Chem. C* **2007**, *111*, 2205−2211.
(34) Sato, K.; Nagaoka, K. Boosting Ammonia Synthesis under Mild Reaction Conditions by Precise Control of the Basic Oxide−Ru Interface. *Chem. Lett.* **2021**, *50*, 687−696.
(35) Watanabe, F.; Kaburaki, I.; Shimoda, N.; Satokawa, S. Influence of nitrogen impurity for steam methane reforming over noble metal catalysts. *Fuel Process. Technol.* **2016**, *152*, 15−21.
(36) Abdel-Mageed, A. M.; Kučerová, G.; Bansmann, J.; Behm, R. J. Active Au Species During the Low-Temperature Water Gas Shift Reaction on Au/CeO_2: A Time-Resolved Operando XAS and DRIFTS Study. *ACS Catal.* **2017**, *7*, 6471−6484.
(37) Ishiguro, N.; Saida, T.; Uruga, T.; Nagamatsu, S.; Sekizawa, O.; Nitta, K.; Yamamoto, T.; Ohkoshi, S.; Iwasawa, Y.; Yokoyama, T.; Tada, M. Operando Time-Resolved X-ray Absorption Fine Structure Study for Surface Events on a Pt_3Co/C Cathode Catalyst in a Polymer Electrolyte Fuel Cell during Voltage-Operating Processes. *ACS Catal.* **2012**, *2*, 1319−1330.
(38) Asakura, H.; Hosokawa, S.; Ina, T.; Kato, K.; Nitta, K.; Uera, K.; Uruga, T.; Miura, H.; Shishido, T.; Ohyama, J.; Satsuma, A.; Sato, K.; Yamamoto, A.; Hinokuma, S.; Yoshida, H.; Machida, M.; Yamazoe, S.; Tsukuda, T.; Teramura, K.; Tanaka, T. Dynamic Behavior of Rh Species in Rh/Al_2O_3 Model Catalyst during Three-Way Catalytic Reaction: An Operando X-ray Absorption Spectroscopy Study. *J. Am. Chem. Soc.* **2018**, *140*, 176−184.
(39) Hinokuma, S.; Wiker, G.; Suganuma, T.; Bansode, A.; Stoian, D.; Huertas, S. C.; Molina, S.; Shafir, A.; Rønning, M.; van Beek, W.; Urakawa, A. Versatile IR Spectroscopy Combined with Synchrotron XAS−XRD: Chemical, Electronic, and Structural Insights during Thermal Treatment of MOF Materials. *Eur. J. Inorg. Chem.* **2018**, *2018*, 1847−1853.
(40) Pan, Q.; Peng, J.; Wang, S.; Wang, S. In situ FTIR spectroscopic study of the CO_2 methanation mechanism on Ni/$Ce_{0.5}Zr_{0.5}O_2$. *Catal. Sci. Technol.* **2014**, *4*, 502−509.
(41) Yoshida, H.; Narisawa, S.; Fujita, S.; Ruixia, L.; Arai, M. In situ FTIR study on the formation and adsorption of CO on alumina-supported noble metal catalysts from H_2 and CO_2 in the presence of water vapor at high pressures. *Phys. Chem. Chem. Phys.* **2012**, *14*, 4724−4733.
(42) Ravel, B.; Newville, M. ATHENA, ARTEMIS, HEPHAESTUS: data analysis for X-ray absorption spectroscopy using IFEFFIT. *J. Synchrotron Radiat.* **2005**, *12*, 537−541.
(43) Damma, D.; Ettireddy, P.; Reddy, B.; Smirniotis, P. A Review of Low Temperature NH_3-SCR for Removal of NO_x. *Catalysts* **2019**, *9*, 349.
(44) Brown, M. F.; Gonzalez, R. D. An infrared study of the adsorption of carbon monoxide on the reduced and oxidized forms of silica supported ruthenium. *J. Phys. Chem. C* **2002**, *80*, 1731−1735.
(45) Davydov, A. A.; Bell, A. T. An infrared study of NO and CO adsorption on a silica-supported Ru catalyst. *J. Catal.* **1977**, *49*, 332−344.
(46) Hadjiivanov, K.; Lavalley, J.-C.; Lamotte, J.; Maugé, F.; Saint-Just, J.; Che, M. FTIR Study of CO Interaction with Ru/TiO_2 Catalysts. *J. Catal.* **1998**, *176*, 415−425.

https://doi.org/10.1021/jacsau.2c00195
JACS Au 2022, 2, 1627−1637

(47) Gupta, N. M.; Kamble, V. S.; Iyer, R. M.; Thampi, K. R.; Gratzel, M. The transient species formed over Ru-RuO_x/TiO_2 catalyst in the CO and CO + H_2 interaction: FTIR spectroscopic study. *J. Catal.* **1992**, *137*, 473−486.
(48) Guglielminotti, E.; Boccuzzi, F. Nitric Oxide Adsorption and Nitric Oxide-Carbon Monoxide Interaction on Ru/ZnO Catalyst. *J. Catal.* **1993**, *141*, 486−493.
(49) Yokomizo, G.; Louis, C.; Bell, A. T. Thermal desorption and disproportionation of CO adsorbed on Ru/SiO_2. *J. Catal.* **1989**, *120*, 15−21.
(50) Yang, S.; Wang, X.; Chu, W.; Song, Z.; Zhao, S. An investigation of the surface intermediates of H_2-SCR of NOx over Pt/H-FER. *Appl. Catal., B* **2011**, *107*, 380−385.
(51) Prins, R. Hydrogen spillover. Facts and fiction. *Chem. Rev.* **2012**, *112*, 2714−2738.

https://doi.org/10.1021/jacsau.2c00195
JACS Au 2022, 2, 1627−1637